



HAL
open science

Combining geodetic and geomorphic methods to monitor restored side channels: Feedback from the Upper Rhine

David Eschbach, Pierre Grussenmeyer, Mathieu Koehl, Samuel Guillemin,
Laurent Schmitt

► To cite this version:

David Eschbach, Pierre Grussenmeyer, Mathieu Koehl, Samuel Guillemin, Laurent Schmitt. Combining geodetic and geomorphic methods to monitor restored side channels: Feedback from the Upper Rhine. *Geomorphology*, 2021, 374, 10.1016/j.geomorph.2020.107372 . hal-03368001

HAL Id: hal-03368001

<https://hal.science/hal-03368001>

Submitted on 2 Jan 2023

HAL is a multi-disciplinary open access archive for the deposit and dissemination of scientific research documents, whether they are published or not. The documents may come from teaching and research institutions in France or abroad, or from public or private research centers.

L'archive ouverte pluridisciplinaire **HAL**, est destinée au dépôt et à la diffusion de documents scientifiques de niveau recherche, publiés ou non, émanant des établissements d'enseignement et de recherche français ou étrangers, des laboratoires publics ou privés.



Distributed under a Creative Commons Attribution - NonCommercial 4.0 International License

COMBINING GEODETIC AND GEOMORPHIC METHODS TO MONITOR RESTORED SIDE CHANNELS: FEEDBACK FROM THE UPPER RHINE

5 David Eschbach^{a,*}, Pierre Grussenmeyer^b, Mathieu Koehl^b, Samuel Guillemin^b, Laurent Schmitt^a

^a University of Strasbourg, CNRS, LIVE UMR 7362, LTSER - "Zone Atelier Environnementale Urbaine", 3 rue de l'Argonne, F-67083 Strasbourg, France (laurent.schmitt@unistra.fr)

10 ^b ICube Laboratory, UMR 7357, Photogrammetry and Geomatics Group, INSA Strasbourg, 24 boulevard de la Victoire, F-67084 Strasbourg, France (firstname.lastname@insa-strasbourg.fr)

* **Corresponding author:** David Eschbach (eschbach.pro@gmail.com). Present address: Sorbonne University, CNRS, EPHE, UMR 7619 Metis, F-75005 Paris, France.

Abstract

15 Producing accurate and rapid geomorphic surveys is a key issue for the growing scientific and operational area of physical river restoration. A geodetic survey using 3-D modeling (lasergrammetry, photogrammetry, tacheometry) was combined with a geomorphic survey (RFID bedload tracking, survey of grain size, geomorphic units evolution and geometrical changes) in order to monitor morphodynamic adjustments in a restored anastomosing channel of the Upper Rhine. On this basis, functioning indicators were developed to survey morphological changes at different spatio-temporal scales. Because

20 Structure from Motion (SfM)-photogrammetry is a fast and low-cost method able to produce high-resolution point clouds, the method is particularly well-suited for monitoring complex fluvial environments that have been subject to rapid and intense changes. A hybrid method was developed to complement bank point-clouds with bathymetric data obtained by Total Station leveling. By using the Multiscale Model to Model Cloud Comparison method (M3C2), volumes of erosion-deposition were determined for all surveys. Combining geodetic and geomorphic approaches resulted in a detailed

25 assessment of channel adjustments. This was achieved by creating a set of indicators (e.g., related to vertical and longitudinal evolutions, sediment budget, etc.) that allowed us to both characterize geomorphic adjustments and identify morphodynamic limiting factors. These indicators may be used in the future in a wide range of restoration surveys.

Key words

Morphological 3-D modelling; Morphodynamic functioning indicators; Sediment budget; Mid-sized river hydro-morphological restoration.

1 Introduction

5 The geomorphic monitoring of restored hydrosystems is a key issue in surveying channel adjustments (Hickin, 1983; Gurnell *et al.*, 2006), habitat dynamics (Raven *et al.*, 2002; Palmer *et al.*, 2010; Belletti *et al.*, 2014) and thereby assessing the efficiency of restoration actions (Fausch *et al.*, 2002; Bernhardt *et al.*, 2005; Stammel *et al.*, 2011; Buchanan *et al.*, 2012; Rinaldi *et al.*, 2017). Conventional morphological surveying techniques, which are usually based on cross sections, are time consuming and require a trade-off between temporal and spatial resolution, accuracy, and survey frequency (Lane *et al.*,
10 1994; Barker *et al.*, 1997; Brasington *et al.*, 2000; Bangen *et al.*, 2014a). The first applications of remote sensing in fluvial environments date back to the 1960s (Painter *et al.*, 1974; Collins and Moon, 1979). However, no significant technological innovations in topographic techniques that would have improved and simplified field surveys appeared before the beginning of the twenty-first century (James & Robson, 2012; Westoby *et al.*, 2012; Nadal-Romero *et al.*, 2015; Smith *et al.*, 2015; Dietrich, 2016; Eltner *et al.*, 2016).

15 Numerous studies have analyzed the accuracy and resolution (Smith *et al.*, 2015; Eltner *et al.*, 2016; Grussenmeyer *et al.*, 2016; Murtiyoso and Grussenmeyer, 2017) of Terrestrial Laser Scanning (TLS; Telling *et al.*, 2017) and Structure from Motion (SfM)-derived topographic datasets for a wide range of geomorphic environments (Table 1). Compared to the first TLS instrument that was developed two decades ago, recent technologies (e.g., FARO Focus 3D, Z+F IMAGER 5016) use smaller, more lightweight devices, and provide high quality colorimetric clouds (Remondino and El-Hakim, 2006). The TLS
20 method is still expensive because of the high cost of the recording system, and that it requires special care in remote areas (targets, spheres, etc.). These constraints explain why only a few surveys aiming at monitoring geomorphic changes in dynamic channels have been based on TLS (Table 1). Besides, SfM photogrammetry is a low-cost method that generates high spatial resolution and 3-D data. It also allows for accurate surveys of frequent river changes, potentially for the short- (<5 yr) and/or mid-term (>5 yr; Fonstad *et al.*, 2013). Additionally, we consider in Table 4 that long-term periods cover >10
25 yr). However, despite the well-known high accuracy of 3-D topographic monitoring obtained by TLS and SfM-

photogrammetry, these methods have been rarely used in river restoration, especially in the context of monitoring morphodynamic changes in side channel restoration (Table 1). Recent geomorphic studies also use newly developed remote sensing applications such as Unmanned Aerial Systems (UAS; Lejot *et al.*, 2007; Casado *et al.*, 2015; Prosdocimi *et al.*, 2015; Woodget *et al.*, 2015; Belletti *et al.*, 2017), tethered kites, blimps (Boike and Yoshikawa, 2003; Smith *et al.*, 2009; Vericat *et al.*, 2009) and near-census approaches to identify and map a wide range of morphological changes at any spatial scale (Wyrick *et al.*, 2014, 2016).

Recent remote sensing applications provide fine Digital Elevation Models (DEM) combined with bathymetric modelling for a large range of channel types (Gao, 2009; Flener *et al.*, 2013; Williams *et al.*, 2014; Eltner *et al.*, 2016). They are, however, limited by water depth, riparian canopy effects, and logjams, which are frequent along dynamic side channels located in dense alluvial forests. Within this context, the combination of survey technologies (e.g., mixing GPS and LiDAR data) is useful to generate complete and accurate datasets (Wheaton *et al.*, 2009; Bangen *et al.*, 2014b). This provides a way to visualize and precisely quantify channel adjustments (e.g., the sediment budgets) by applying DEM of Difference (DoD) (Martin and Church, 1995; Brasington *et al.*, 2000a; Lane *et al.*, 2000; Wheaton *et al.*, 2009; Milan, 2012; Wyrick *et al.*, 2016).

With the increased number of river restoration projects during the last three decades (Morandi *et al.*, 2014), many studies tried to develop indicators that would allow assessing the efficiency and sustainability of such management actions (Berger, 1997; Palmer *et al.*, 2005; Brierley and Fryirs, 2008; Dufour and Piégay, 2009; Pander and Geist, 2013; Rinaldi *et al.*, 2017), but only a few studies have combined geodetic surveys and conventional geomorphic methods (McLean and Church, 1999; Chandler *et al.*, 2002; Chapuis *et al.*, 2015; MacVicar *et al.*, 2015). An indicator in fluvial geomorphology is a quantified specific metric allowing the characterization of the evolution of fluvial forms (generally in longitudinal, lateral and/or vertical dimensions) and processes (erosion, sediment deposition, bedload dynamics; Corbonnois *et al.*, 2011). The global objective of the paper is to assess the impacts of a restoration project (morphological changes, bedload dynamics, habitats diversification, etc.) by combining geodetic (TLS, SfM) and geomorphic monitoring methods. More specifically, a threefold aim is targeted in the framework of the functional restoration performed in the Rohrschollen island (Upper Rhine River, France): (i) to adapt geodetic survey to monitor intense and frequent morphological changes along a dynamic side channel,

- (ii) to combine this geodetic survey with classical geomorphic methods to develop a set of morphodynamic indicators and
- (iii) to interpret results in terms of efficiency and sustainability of the restoration project.

Authors Date	Context	Approach	Geomorphological dimensions & components										DEM methods		Hydromorphological methods						
			Channel types	River restoration	Lateral channel restoration	Geomorphological survey	Methodological studies ^a	Lateral adjustments	Vertical adjustments	Bedload dynamics	Hydrodynamics	Geomorphic units evolution	Lasergrammetry	Photogrammetry	Levelling (cross-section)	RFID tracking	Hydraulic modelling	Sediment budget	Other methods		
Collins and Moon, 1979	WR																				
Dickinson and Scott, 1979	MR																				
Lane et al., 1994	BR																				
Martin and Church, 1995	BR																				
Barker et al., 1997	MR																				
Pyle et al., 1997	PGR																				
Heritage et al., 1998	MR																				
Westaway et al., 2000	BR																				
Brasington et al., 2000	BR																				
Chandler and Shiono, 2001	TF																				
Lane et al., 2001	TF																				
Chandler et al., 2002	PGR																				
Fuller et al., 2003	WR																				Bar
Formann et al., 2007	BR																				Bar
Lejot et al., 2007	BR																				Bar
Wheaton et al., 2009	BR																				Bar
Lague et al., 2013	MR																				
Bangen et al., 2014a	SAC																				
Javernick et al., 2014	BR																				
Casado et al., 2015	WR																				
Chapuis et al., 2015	WR																				
Kuo et al., 2015	BR																				
MacVicar et al., 2015	SAC																				
Brunier et al., 2016	BR																				Bar
Dietrich, 2016	SAC																				
Jozkow et al., 2016	MS																				
Belletti et al., 2017	WR																				
Marteau et al., 2017	MS																				
Cook, 2017	WR																				
Wyrick et al., 2016	WR																				
Jugie et al., 2018	SAC																				

BR Braiding River
SAC Small Alluvial Channel
TF Tilting Flume
MR Meandering River
MS Mountain Stream
PGR ProGlacial River
WR Wandering River

^a Results focused on methodological innovation (accuracy, methodological comparison...)
^b Bathymetric models
^c Unmanned Aerial Vehicles (UAV) and Artificial Neural Networks (ANN)
^d Geomorphic Units Survey (GUS) and Morphological Quality Index (MQI)
^e Near-census approach and decision-tree classification
^f Photo-Electronic Erosion Pin (PEEP)

Table 1: Studies developed to monitor geomorphic channel changes by using DEM approaches.

2 Study site

The Rohrschollen artificial Island is located about 8 km South East of the City of Strasbourg (Fig. 1a). It results from the construction of a power plant on the Rhine canal in 1970 (Fig. 1b). It has been highly impacted by engineering works since the beginning of the nineteenth century (Eschbach *et al.*, 2018). A diversion dam located at the southern side of the island (Fig. 1b) divert up to $1550 \text{ m}^3 \cdot \text{s}^{-1}$ towards the power plant by means of an artificial canal (named “Rhine canal”). When discharge is below this threshold, only $13 \text{ m}^3 \cdot \text{s}^{-1}$ feed the Old Rhine (East part of the island; Fig. 1b). When the Rhine discharge exceeds $1550 \text{ m}^3 \cdot \text{s}^{-1}$, overflows are streamed into the Old Rhine. The agricultural dam located in the northern side of the island allows progressive floods when discharges exceed $2800 \text{ m}^3 \cdot \text{s}^{-1}$ (CIPR-ICPR, 2012). Consequently, during floods, the island is submerged by static flow. Significant flood retention rarely occurs, about once per decade in average. In addition, flowing water during floods does not occur and active morphodynamic processes in the floodplain and the anastomosing channel of the island. In this study, this channel is called “old channel” (Fig. 1b).

In the framework of the European LIFE+ project, launched in 2012, a floodgate was constructed, as well as a stabilized rockfill canal and a new upstream non-stabilized channel (called “artificial side channel”), which were excavated in the southern part of the island to reconnect the old channel to the Rhine’s hydrological regime. Depending on the discharge of the Rhine, water injected by the floodgate ranges from 2 to $80 \text{ m}^3 \cdot \text{s}^{-1}$ during an average of about 51 days annually when the Rhine discharge is higher than $1550 \text{ m}^3 \cdot \text{s}^{-1}$. This new mode of functioning should allow the reestablishment intense and frequent morphodynamic processes (bank erosion, bedload transport, etc.), especially in the artificial side channel, which was intentionally undersized to induce self-forming adjustments. The artificial side channel shows a mean longitudinal water slope of 0.94‰, a bankfull discharge of about $20.5 \text{ m}^3 \cdot \text{s}^{-1}$, a mean bankfull width of about 12 m (except on sector C; see Section 3.1) and a mean initial bankfull specific stream power of $15\text{-}22 \text{ W} \cdot \text{m}^{-2}$ (February 2014).

Fig. 1 (Study_site)

Figure 1: (a) Location of the Rohrschollen Island in the Upper Rhine basin, (b) DEM of the whole study site and location of the main engineering works, (c) three survey sectors located on curvatures of the artificial side channel (white linear), (d) pictures of the diachronic evolution close to the three curvature sectors, (e) hydrogram of the reporting period.

5 3 Material and methods

3.1 Experimental spatial and flow regime designs

Our investigations focused on two spatial scales: (1) the whole artificial side channel and (2) three curvature sectors of this channel corresponding to reaches where lateral erosion was expected to be the highest (noted A, B and C in Fig. 1c). The morphological evolution of the old channel will not be discussed in this paper. Short and low intensity ecological floods were conducted during summer 2014 (less than $20 \text{ m}^3 \cdot \text{s}^{-1}$ during about 1-2 h; see the top of the Fig. 2: trial flow pulse). Several ecological floods occurred during May and June 2015. Two main experimental floods were designed (Fig. 1e). Flood 1 was based on an incremental progress with three sporadic peaks in order to test the floodgate ($40\text{-}70 \text{ m}^3 \cdot \text{s}^{-1}$) and flood 2 was characterized by a high discharge of $60 \text{ m}^3 \cdot \text{s}^{-1}$ during 48 h (in accordance with the discharge of the Rhine). Diachronic pictures in Fig. 1d illustrate the effects of floods (enlargement, lateral erosion, bar formation, etc.) in the vicinity of the three studied curvature sectors during the total survey period. The total period covers two morphological changes (called surveying periods in Fig. 2) highlighted by three states that resulted from flood events that occurred from February 2014 to March 2016 (Fig. 2).

3.2 Geodetic survey

3.2.1 TLS and SfM comparison

20 Focusing on the three main curvature sectors of the artificial side channel (Fig. 1c), the initial post-restoration state (state 0 = before floods and morphological evolution) was recorded before the first floods by a combination of TLS and SfM methods. TLS was set up with a FARO Focus 3-D with complete vertical and horizontal 360° view. This system can deliver an accuracy of 2 mm at 25 m. The system was setup to provide a spatial sampling of 3 mm at 10 m (Faro resolution setting: $\frac{1}{2}$). Photogrammetric images were recorded using a calibrated Canon EOS 5D Mark II camera with a focal length of 28 mm. The camera was fixed on a tripod and translated along the riverbanks to satisfy a forward overlap of 70-80% between the successive parallel images. Additional oblique images were recorded to improve the geometry of the photogrammetry

datasets. Circular coded control targets permanently fixed on trees and regularly distributed on both riverbanks were used to process the images and georeference each curvature sector. To avoid errors related to the movement of trees (e.g., tree growth), the XYZ data of each target were collected at least once a year, if possible, during the SfM acquisition. Dense point clouds (Medium quality setting, i.e., ~1 pt/cm after post-processing) were generated using the *Photoscan* SfM software (version 1.2.6) and the optimization tool was used to georeference each sector. The internal projection errors for the GCPs were less than 5 cm and below 0.5 pixel (Table 2). The accuracy of the SfM method was assessed by a cloud to cloud registration algorithm considering TLS as a reference. Cloud to cloud accuracy ranged from 2 to 5 cm. The SfM method was therefore considered satisfactory and well-suited to monitor important morphological adjustments and rapid changes in the three curvature sectors.

10

	Sector A		Sector B		Sector C	
	Left bank	Right bank	Left bank	Right bank	Left bank	Right bank
Number of image	128	90	129	101	74	83
Number of GCP	5	6	7	8	10	7
Reprojection error (Standard deviation m)	0.001	0.02	0.02	0.05	0.03	0.01
Reprojection error (Standard deviation pixels)	0.18	0.23	0.49	0.2	0.19	0.12

Table 2: *Photoscan* parameters for each sector. Example for state 2 (March 2016).

3.2.2 Topographical data

A Total Station recording was used to detect morphological changes beneath the water surface, as proposed by Lane *et al.* (1994), and beyond the water between the curvature sectors. Regularly spaced (20 m) cross sections composed of 5 to 8 points were recorded in XYZ along the whole artificial side channel. Supplementary thalweg points were collected between each cross section for the longitudinal profile. In fact, such a method is time-consuming and can only generate a relatively small set of bathymetric points (Chandler *et al.*, 2002), but provides a reliable terrain-modeling method to quantify changes at the scale of the whole channel (Brasington *et al.*, 2000). Differential GNSS positioning was used to set up reference points upstream and downstream of the channel (Leica TS02 Total Station and Leica GPS 1200 System used in GNSS RTK Mode). They were connected with the polygonal network in order to provide a comparable diachronic database. Planimetric and

20

altimetric accuracy were about 3 cm. Thalweg trajectories were extracted using the free extension to the desktop *ArcGis* software from ESRI “River bathymetry Toolkit” with a 0.5 m vector resolution (ESSA, 2016).

3.2.3 Point cloud comparison

For each sector, accurate TIN models based on the dense point clouds were merged with DEM bathymetric data to generate
5 “combined models”. The *CloudCompare M3C2* (version 2.8.1) method was used to record differences between point clouds from two consecutive surveys (Lague *et al.*, 2013; Fig. 2). The normal-scale parameter has been set to 1-2 m. We consider this parameter satisfactory to average the topographical discontinuities of the riverbanks. To provide a reliable comparison of high morphological volume changes (especially with regards to lateral erosion), a gridding interpolation was defined before merging two point clouds. Finally, a script implementation based on *MatLab* functions developed by TRIO group was used
10 to calculate volume differences automatically between two clouds at two spatial scales: the whole channel and the three sectors.

3.3 Geomorphic survey

3.3.1 Grain size survey

To characterize the grain size at the channel bottom, the Wolman (1954) method was used on bars, riffles and an inherited
15 gravel bar exhibiting particularly coarse grain sizes. Homogeneous grain size patches were delimited and b-axis measurements of 100 particles on each patch were taken, as recommended by Kondolf *et al.* (2016). This was used to generate grain size cumulative curves and extract statistical parameters such as the median diameter and standard deviation.

3.3.2 RFID tracking

The method involves attaching passive Radio Frequency IDentification (RFID) tags into gravel particles in order to track
20 bedload movement (Lamarre *et al.*, 2005). We employed low-frequency tags consisting of glass cylinders 3.8 mm in diameter and 23 mm in length operating at 134.2 kHz and distributed by Texas Instruments (TI-RFID, 2006). A total of 413 particles with a b-axis of 22.6 to 64 mm were instrumented. RFID tags were attached to each particle by creating a lateral notch for the smaller particles and by drilling into the larger particles. Implementation was realized before state 1. Tracers were distributed homogeneously between the three transects at three injection-points located on both sides and in the middle

of the channel bottom. The experiment took place during two periods: the first one occurred between the two ecological floods of surveying period 2 and the second one was performed during state 2 (Fig. 2).

During field surveys, bars and shallow-water areas were monitored on foot using a 0.46 m diameter loop antenna and tracer positions were recorded using a GPS Trimble 6000 GNSS RTK. An accuracy of 0.05 to 0.10 m for such GPS points was reached after post-processing. In addition, horizontal errors include the detection limit of the antenna of around 0.34 m. Maximum cumulative horizontal errors were estimated to be ± 1 m depending on the relative position of the antenna during the survey, RFID orientation and GPS survey (Schneider *et al.*, 2010; Chapuis *et al.*, 2014; Arnaud *et al.*, 2015). According to operating controls carried out by Arnaud *et al.* (2015), the vertical detection error for the 0.46 m detection system is about 0.69 m. Mean tracer recovery rate attained 41% after the first flood and decreased to 31% for state 2. Transport distances were calculated automatically by applying the vectorization function in *ArcGis 10.3* to relay starting and ending points corresponding to the GPS points of each particle between two floods. Displacement trajectory was improved manually by using the thalweg pattern.

3.3.3 Geomorphic unit survey

Following Malavoi and Souchon (2002) and Schmitt *et al.* (2011), the channel was divided into different in-channel Geomorphic Units (GU): riffles, pools, and runs. Bars were added as a GU because they represent an important ecological habitat for pioneer alluvial vegetation. Surveys were conducted during low flow. Points were recorded by GPS RTK to localize the main limits between each GU. Aerial images, acquired during state 1 for another study (Eschbach *et al.*, 2017), were used to improve the delineation. For state 2, we used a ground control photographic interpretation as well as longitudinal and transverse profiles to improve the delineation between units. For each surveyed state, GU surfaces were measured using the “compute geometry” function in *ArcGis 10.3*. In addition, logjams were located for each state. No survey was implemented for state 0 because of the artificial state of the channel (no water, no natural fluvial forms like pool-riffle sequences, bars, etc.).

3.3.4 Survey of lateral and vertical adjustments

Lateral channel mobility for each sector was determined using a sinuosity index that was calculated by using state 0 as the reference situation. An indicator of bankfull geometry evolution was calculated using the width/depth ratio (Schmitt *et al.*, 2007) and the lateral erosion rate (I_{ler} ; Fig. 2) mentioned by Malavoi and Bravard (2010). The latter corresponds to the eroded width between two floods (w_e) divided by the width at the initial stage of the surveyed event (w_{in}), as shown in the following formula:

$$I_{ler} = \left[\frac{w_e}{w_{in}} \right] * 100 \quad (1)$$

To analyze vertical adjustment between the two states, we developed an indicator of thalweg vertical variation (I_{vv} ; Fig. 2) by calculating positive residuals (R^+) and negative residuals (R^-) between the second longitudinal profile (state 2) and the straight trend line of the first longitudinal profile (state 1). Thalweg aggradation of the longitudinal profile is marked by $\Sigma R^+ > \Sigma R^-$. Conversely, $\Sigma R^+ < \Sigma R^-$ indicates thalweg incision. The thalweg longitudinal variability was calculated using the standard deviation of the residuals of both surveys (I_{vv}).

Fig. 2 (Methods)

Figure 2: Top: details of the hydrological events during the reporting period and features of fieldwork acquisition for the two states. Bottom: process workflow (grey arrows) and results produced to achieve a global hydromorphological understanding of the channel functioning. Because the artificial side channel did not show any natural fluvial forms (i.e., pool-riffle sequences, bars, etc.), only the topographic and grain size surveys were used for State 0.

4 Results

4.1 Multiscale sediment budgets (I_q)

4.1.1 Sediment budget close to the three curvature sectors

Comparisons between the 3-D combined models are locally affected by data gaps (white holes in Fig. 3a), which results from removing of riverine vegetation and logjams during data processing. However, the colorimetric visualization of diachronic evolutions based on cloud to cloud comparisons allowed us to locate and quantify accurately erosion versus deposition processes at the channel boundaries. Suspended load was determined for 10 L of water sampled in the middle of the channel during an ecological flood (the upstream part of the water column was sampled).

After the first short and low-intensity hydrological trial flow pulse (surveying period 1, top of the Fig. 3a), the bottom of the channel in the three curvature sectors showed little morphological changes (i.e., vertical dynamics). Lateral dynamics were more pronounced, especially on concave banks (locally bank erosion reached up to 2 m; Fig. 3a, sectors A and B) and on convex banks where deposition (formation of convex bars) attained up to 1.5 m (sectors A and B). Volumes of deposition (D) reached 131.3 ± 16 and 268.7 ± 15 m³ on sectors A and B, respectively, while volumes of erosion (E) attained on these sectors were 246.1 ± 16 and 225.6 ± 26 m³, respectively (Table 3). Sector C recorded the most important adjustments, with maximum erosion-deposition attaining 2.5 m. Similarly, volumes of erosion (E) in this sector were more than two times higher than for sectors A and B (Fig. 3a). I_q abstracted from sediment budgets indicates that the deposition volume (D) at sector C is 171 m³ higher than at sector 1 and 33 m³ higher than at sector B. Additionally, sediment output (O) reached 235.8 ± 22 m³ in sector C while being twice as low in sector A (114.8 ± 22 m³) and zero in sector B (because deposition was 43.1 ± 14 m³ higher than erosion).

Comparison between state 2 and state 1 (surveying period 2) shows an intensification of erosion in sectors A and B (from 131.3 ± 16 to 166.5 ± 26 m³ and from 225.6 ± 16 to 310.0 ± 26 m³, respectively; Table 3). Compared to state 1, the lengths of lateral erosion were shorter, while channel scouring at the feet of concave banks was longitudinally more extended, as were deposition areas in convex banks. Although eroded volumes have increased in the two upstream sectors (A = $+26 \pm 15$ m³ and B = $+84.4 \pm 26$ m³), deposited volumes were higher in sector A (35.2 m³) and stayed stable in sector B (-0.7 m³; Table 3). In sector C, erosion prevails over deposition, which is locally present in the downstream part of the sector. The sediment budget in this sector shows the same tendency, with a large differential between erosion (245.6 ± 28 m³) and deposition (66.5 ± 12 m³), but this trend significantly decreased in comparison with surveying period 1.

Sector A	SP1	SP2	<i>Diff.</i>
Deposition (D)	131,3	166,5	35,2
Output (O)	114,8	105,6	-9,2
Erosion (E)	246,1	272,1	26

Sector B	SP1	SP2	<i>Diff.</i>
Deposition (D)	268,7	268	-0,7
Output (O)	0	42,7	42,7
Erosion (E)	225,6	310	84,4

Sector C	SP1	SP2	<i>Diff.</i>
Deposition (D)	302,1	66,5	-235,6
Output (O)	235,8	176,2	-59,6
Erosion (E)	537,9	245,6	-292,3

Table 3: Volumes (m³) of sediment deposited, eroded and output from the three sectors.

4.1.2 Sediment budget along the whole channel

At larger temporal (surveying periods 1 and 2) and spatial scales (the whole channel; Fig. 3b), cumulative erosion and deposition curves show no differentiation until 200 m on the x-axis (distance from the beginning of the channel). This distance is the transition point between the rockfill canal and the artificial side channel (Fig. 5e). From this point on, the differential between erosion and deposition rapidly reaches 500 m³, before reaching 750 m³ in sector A. The erosion curve is characterized by three main growth phases corresponding to the three curvature sectors (concave bank erosion). The main one is included in the upstream part of sector C (x = 850 m; Fig. 3b). Cumulative volume of eroded sediment reached up to 3500 m³ downstream of the whole artificial side channel (x = 1050 m; Fig. 3b). The deposition curve is logically below the curve for erosion, but follows the same general longitudinal tendency. The three major deposition growth peaks are spatially shifted almost 50 m downstream of the erosion growth peaks, excepted for sector B where the deposition curve is almost parallel to the erosion curve. The final difference in values between the two cumulative curves is up to 1000 m³, which represents the volume of fine sediments (part of sand, silt, clay) exported towards the old channel, the floodplain and the Old Rhine.

Based on surveying period 2, at the scale of the whole channel, we determined specific sediment budgets (m³) for each type of component of the channel boundaries (m²): morphological bank types (straight, concave, convex) and channel bottom (Fig. 5b.). Consequently, sediment budgets for this analysis are expressed in m³/m² (Fig. 5b). These results are based on comparisons of elementary reaches and allowed the linking of vertical and lateral volumetric evolutions. It appears that erosion is higher for banks than for the channel bottom, with a maximum volume of lateral erosion that could attain 0.26 m³/m² (x = 400 m), while vertical evolution does not exceed 0.05 m³/m² (x = 390 m). This tendency not only affects the concave banks, but also the straight banks, locally impacting the entire cross section, including also convex banks (especially

in sector C). Conversely, deposition logically occurs mostly at the channel bottom, and locally on banks (convex but also locally concave banks). In addition, it is worth noting that lateral and vertical erosion-deposition volumes are significantly low between 500 and 650 m.

Fig. 3 (Results_BS)

5 **Figure 3: (a) Comparison of 3-D combined models using M3C2 during both surveying periods on the three curvature sectors, including sediment budgets. (b) Global cumulative sediment budget for the whole channel during both surveying periods.**

4.2 Lateral channel evolution (I_{ler})

In the three curvature sectors, the position of the thalweg shifted locally up to 7 m towards concave banks, while mean relative sinuosity increased from 1.0 to 1.05. This indicates curvature accentuation band concave bank erosion and the lateral
10 migration of the thalweg during floods (Schumm, 1968; Fig. 4a). Bankfull surfaces tended to converge over the two periods to between 18.60 and 20.89 m² (Fig. 4c). Widths increased in all cross sections, especially in CS22 (+1.67 m; +16%) and CS34 (+4.39 m; + 52%). The W/D ratio increased from 5.68 to 7.61 in CS7, from 4.55 to 7.68 in CS22, and from 3.77 to 8.96 in CS34. Lateral erosion (I_{ler}) was very low for CS7 with a value of 0.3% during the surveying period 1 and 2.5% during the surveying period 2. For CS22, lateral erosion increased from 6.1% to 9.2% between the two surveying periods.
15 CS34 recorded the highest lateral erosion related to the first surveying period (44.2%) followed by a lowest value (5.0%) for the second surveying period.

Fig. 4 (Results_LER)

Figure 4: Examples of lateral channel evolution in the three curvature sectors, with (a) thalweg evolution, (b) examples of diachronic cross sections, (c) resulting indicators of lateral channel evolution (I_{ler}) and bankfull specific stream power.

20 4.3 Vertical variation (I_{vv})

The comparison of longitudinal profiles during surveying period 2 (Fig. 5e) allows the identification of thalweg vertical variations, characterized by aggradation sectors that correspond notably to riffles (e.g., x = 240; 290; 500; 980 m) and scour sectors that correspond to pools (e.g., x = 225; 260; 425; 725; 875 m). A stable sector, covering mostly sector B, was identified, extending from 530 m to 700 m. No logjams are located between 425 and 830 m. In fact, these are especially
25 located in the curvature sectors A and C (Fig. 5e). These sectors are also characterized by high vertical evolution, mostly erosion.

Results of the global longitudinal evolution (I_{vv}) reveal a longitudinal reversal characterized by three main tendencies (Fig. 5a). The first sector is characterized by a thalweg incision tendency that extends from 225 m to 510 m ($\Sigma R^+ < \Sigma R^-$). Low cumulative residual variations between 510 m and 645 m indicate vertical stability. Conversely, the thalweg is characterized by an aggradation tendency between 645 m and 1150 m. The thalweg longitudinal variability shows an important
5 augmentation in the difference, from original values around 0.1 for the whole channel at state 0. Comparison between state 1 and 2 shows that the difference increased to 0.15 - 0.41 and 0.15 - 0.28, for the upstream and downstream sectors, respectively. By contrast, these values remained around 0.1 in the identified stable sector.

4.4 Evolution of geomorphic units (I_{gu})

The evolution of geomorphic units was surveyed to assess gain or loss of habitat diversity. The total area covered by all
10 geomorphic units increased from 10 000 to 12 520 m² between the two surveys (+25.2%; Fig. 5g). This tendency reveals a general channel enlargement (from 2 to 4 m on average). Among the four geomorphic units: riffle, pool, run and bar, major growth of +1100 m² occurred for runs (18.83%). Pools increased by +550 m² (60.5%), closely followed by riffles (+450 m²; 30.5%) and bars (+420 m²; 23.74%).

4.5 Grain size variation and bedload dynamics (I_{bd})

15 With regards to the combined grain size results from the two surveying periods (Fig. 5c), we observed an average D_{50} of 15.3 ± 5 mm, except for samples located at a longitudinal distance of 576 and 602 m where D_{50} is higher than 50 ± 15 mm (standard deviation). Indeed, this sector exhibits a significantly coarser grain size resulting from a large median in-channel gravel bar inherited from past Rhine dynamics, as revealed by the historical study (Fig. 5f; Eschbach *et al.*, 2018). The gravel bar extends from 530 to 815 m under the artificial side channel, and outcrops in the riverbed between 530 and 675 m.
20 Results of RFID tracking are given on Fig. 6 and used as an indicator for bedload dynamics (I_{bd}). According to Lamarre and Roy (2008) and Milan and Large (2014), tracers travel distances recorded in the first survey (S1) are not representative because of an overexposure phenomenon caused by particle setup. This phenomenon is well known and explains why the particles move more easily during the first flood. The results of the two survey periods do not show any significant link between transport distances and particle grain size, indicating a non-selective mobility. The distribution of tracer clouds is

relatively homogeneous through time at transect 8 as well as for survey 1 in transect 9 (Fig. 6b). A significant decrease in travel distances is observed for survey 2 (S2) at transect 9 (Figs. 5d and 6). At this location, mean transport distances drop down from 24.2 to 12.4 m while they increase in transect 8 (from 24.7 to 31.5 m; Fig. 6a). Fig. 6c shows a significant decrease of cumulative distances for transect 9 while they increase in transect 8. This figure shows also that some tracers are slowed down by riffles. By contrast with the recovery rate recorded for transects 8 and 9 (47% and 46%, respectively), the rate for transect 10 (6.5%) is very low, which dampens the robustness of results. Nevertheless, it can be noted that mean transport distances for this transect tended to decrease, from 26.8 to 17.6 m. Results were summarized on Fig. 5d and, to improve readability, consider cumulative travel distance according to the grain size of the tracers.

Fig. 5 (Results_PL)

10 **Figure 5: Longitudinal evolution between (a) vertical variation of cumulative residuals (every 10 m), (b) sediment budget by bank types and channel bottom (every 20 m), (c) grain size, (d) bedload mobility, (e) longitudinal profile evolution, (f) inherited sediment deposits, and (g) geomorphic units evolution.**

Fig. 6 (Results_PIT)

15 **Figure 6: (a) Box-plots of tracer travel distances for the two surveying periods. (b) Travel distances of tracers detected during both surveying periods and according to the grain size of RFID particles. (c) Frequency distribution of the particles location at state 1 and state 2 linked with the evolution of the thalweg longitudinal profiles.**

5 Discussion

5.1 Combining geodetic and geomorphic methods to survey restored river dynamic side channels

20 Although TLS and SfM photogrammetry methods are able to generate high spatial resolution 3-D data to survey bank erosion, the point clouds obtained must be completed by bathymetric surveys to produce complete 3-D models, which can be chronologically compared. Bathymetric changes can be monitored by a set of cross sections generated by Total Station and GPS measurements, but this low resolution method is time-consuming (Lane *et al.*, 1994; Barker *et al.*, 1997; Brasington *et al.*, 2000a; Bangen *et al.*, 2014b). For instance, covering 1 km length of an artificial side channel with cross sections spaced every 20 m and composed each of 5 to 7 leveling points, requires six people during one to two days, depending on field constraints (riparian vegetation, logjams, weather, etc.). During surveys, the positions of topographic points are accurately determined to reveal lateral slope changes, as recommended by Ferguson *et al.* (1992) and Lane *et al.* (1994). Topo-bathymetric surveys are usually used to infer geomorphic features such as longitudinal profiles and cross sections, and to

delineate geomorphic units (riffles, pools and runs). In addition, diachronic topographic points allow the determination of geomorphic changes with an acceptable resolution along reaches (~0.5 – 1 m). Consequently, hybrid methods based on SfM-photogrammetry and Total Station surveys is a relevant compromise between a spatial resolution that is both satisfactory for managers and allows geomorphic interpretation, and field constraints (Westaway *et al.* 2003; Rayburg *et al.* 2009; Legleiter 5 2012; Bangen *et al.* 2014a), especially to survey dynamic side channels.

The major limitation of 3-D modeling applied to a fluvial context is the presence of dense riparian vegetation and logjams, which may partially cover banks and generate gaps in point clouds. To avoid this constraint, we recommend carrying out surveys during winter, when vegetation is the least developed. Furthermore, to survey intra-annual changes and improve stereoscopic pair acquisition (especially when vegetation is high and where numerous logjams are present in the channel), 10 we recommend combining terrestrial and local aerial photogrammetry obtained using drones (Lejot *et al.*, 2007; Raclot *et al.*, 2005), UAV-Photography (Flener *et al.*, 2013) or L-shaped bracket (Grussenmeyer *et al.*, 1996). However, although this method is effective for geomorphologic monitoring of rugged terrain, it is difficult to implement at large spatial scales (more than one kilometre). Its deployment is optimal for sections of a few hundred meters. Beyond this, the acquisition and processing time would become excessively high.

15 Concerning the process workflow, our study shows that the M3C2 method is a powerful tool to visualize morphological changes and to produce detailed sediment budgets at different spatial and temporal scales. However, in the curvature sectors, we recommend anticipating, as much as possible, future lateral evolution so that the area of lateral channel mobility is included into the point cloud scene.

Despite the implementation constraints in alluvial artificial side channels (dense riparian vegetation, accessibility), it seems 20 promising to explore the potential of topographic/bathymetric Light Detection And Ranging (LIDAR) to survey morphological changes at larger spatial scales (Brasington *et al.*, 2000; Legleiter, 2012; Bizzi *et al.*, 2016). In reaches where the water depth is less than 2 m and the turbidity is low, this method has great potential, especially to improve the resolution of bathymetric point clouds (Gao, 2009; Flener *et al.*, 2013; Lague *et al.*, 2013; Woodget *et al.*, 2015).

5.2 Spatio-temporal adjustments identified by using functioning indicators

Main changes were identified in the downstream part of the channel (sector C) where the width was lower (Fig. 1d, sector C in 2014). This induced a high value of stream power (22.2 W.m^{-2}) explaining why morphological changes, especially enlargement, were the highest in this sector (Fig. 3a, sector C, surveying period 1). In comparison, stream power was lower
5 farther upstream (sectors A and B), between 15.4 and 18.1 W.m^{-2} (Fig. 4c). For the survey period 2 (2015-2016), eroded and deposited volumes are slightly more important in sectors A and B but decreased significantly in sector C by comparison to the first survey period (2014-2015). This may be explained by the fact that, for sector C, stream power dropped to about
10 15 W.m^{-2} , which is close to the stream power values of sectors A and B, while for the latter sectors the stream power drop was very low (Fig. 4c). Despite a negative sediment budget for the downstream part of sector C (Fig. 3a, sector C, survey
15 period 2 and Fig. 5b), I_{vv} reveals a general tendency of thalweg aggradation (Fig. 5a). This is especially because of the high lateral enlargement that supplied gravel and induced sedimentation on the channel bottom. Locally, both bank erosion and vertical evolution are also strongly linked to the presence of numerous logjams (Fig. 5e).

Although only short floods occurred during the trial period (survey period 1 - 2014-2015) with a moderate initial bankfull stream power of about 15 to 22 W.m^{-2} , the channel experienced important morphological adjustments. Part of this result is
20 explained by the fact that the channel was newly excavated and featured no sediment sorting as, e.g., surface pebble/gravel pavement. In absence of upstream bedload inputs, I_q revealed that bank erosion provided large bedload volumes into the channel, especially in concave and straight banks (Fig. 5b). While fine sediments are exported out of the channel towards the old channel, the adjacent floodplain and/or the Rhine (Fig. 3b), mean bedload transport distances and dispersion are relatively low at around 20 m and 85 m, respectively. Consequently, coarse sediment inputs by lateral erosion are deposited
25 into the channel and contributed significantly to the diversification of the geomorphic units (I_{gu} ; Fig. 5g), as also shown by Eschbach *et al.* (2017) and studies on other rivers (Hassan *et al.*, 2017; MacWilliams *et al.*, 2006; Sear 1996). On the other hand, diversification of fluvial forms (lateral or median bars, riffles) controlled gravel mobility, as was also showed by Chardon *et al.* (in revision) in the Old Rhine. At transect 8, gravel was trapped in a large pool and in the upstream part of a riffle (Fig. 6c, x-axis = 450 to 470 m). By contrast, travel distances decreased in transect 9 (from 24.2 to 12.4 m) while the
longitudinal profile, as revealed by I_{vv} (Fig. 5a), showed no important changes (Fig. 5e). This results from the presence of the

old bar formed by coarser sediments (mean b-axis size is 50 mm; Fig. 5c), which crops out on the channel bottom and the banks, close to transect 9 (Fig. 5f, between 530 and 675 m). A significant part of PIT tags remained trapped in the pavement for state 2, regardless of the particle size (Fig. 6c). This inherited bar also significantly influenced all morphodynamic indicators, including bedload transport. On the one hand grain size is 2.5 higher than the one along the channel (bottom and bank footslopes) and controls both vertical (I_{vv} ; see stability sector in Fig. 5a) and lateral evolution (I_{ler} ; see bank erosion in Fig. 5b). On the other hand, bedload transport of all grain size classes is considerably lower (I_{bd} ; Fig. 5d). The second specific sector is located in the upstream part of the artificial side channel, directly downstream of the “*Rockfill canal*”. It is characterized by the presence of a sandy palaeochannel, explaining the predominance of sand in both banks and the channel bottom, thereby favoring lateral and vertical erosion (see Fig. 5f, between 190 and 245 m). This is highlighted by the comparison of longitudinal profiles (Fig. 5e) and by the I_{vv} indicator (Fig. 5a) which showed the formation of an important scour pool (Fig. 5e). This is also enhanced by a coarse sediment deficit in this upstream extremity of the channel, linked to the absence of bedload input at the floodgate.

The set of functioning indicators listed in Table 4 summarizes the evolutionary trends that occurred in the artificial side channel of the Rohrschollen Island. Initial restoration state refers to the survey campaign that took place immediately after the digging of the artificial side channel and before the first ecological floods (see “Initial State” column in Table 4). The state “targeted” is based on the restoration objectives defined by the manager and scientists working on the restoration environmental monitoring. This highlights the fact that it is essential to define (quantifiable) objectives for restorations using the same indicators than for post-restoration monitoring (Pander and Geist, 2013; Stammel *et al.*, 2011), as well as for the pre-restoration survey. Results of each indicator developed in the present study are summarized by arrows determining the observed evolutionary trends (see “Post-Resto” column in Table 4). Identified long-term trends are based on the interpretation of results presented in this paper and on the historical study developed in Eschbach *et al.* (2018). Table 4 highlights the systematic increase of all indicators, reflecting the significant morphological diversification that occurred during the first two years following the restoration. Obviously, our results currently reflect post-restoration transitory adjustments, which were exacerbated in the newly excavated, undersized, side channel. This tendency should decrease in the coming years when a dynamic equilibrium will be reached. This research will be continued with additional surveys to

confirm the observed trend. In this study, we mainly focused on geomorphological indicators, but ecological indicators should also be considered to assess the “dynamic equilibrium” targeted by the project, as shown for instance by Woolsey *et al.* (2007), Nielsen and Jorgensen (2013) or Pander and Geist (2013).

INDICATORS	NAME	METRICS	METHODS	State		Evolutionary trend	
				Initial state	Target	Post-Resto ^o	Long-term Target
Geomorphic units evolution	I_{gu}	Surfaces of geomorphic units (habitats)	Mapping of riffle, pool, run, logjams (GPS; ArcGis)	-	+	↗	→
Bedload dynamics	I_{bd}	Transport distances and dispersion	RFID tracking	o	+	↗	→
Vertical variation	I_w	Vertical evolution trend	<ul style="list-style-type: none"> Thalweg longitudinal profile Cumul of the residuals 	-	+	↗	→
Lateral erosion	W/D I_{ler}	Width/depth ratio $I_{ler} = \left[\frac{w_e}{w_{in}} \right] * 100$		Cross section (Total Station)	-	+	↗
Sediment budget	I_q	Volumes (differences) of eroded and deposited sediments	TLS/SfM-photogrammetry/Total Station and DoD	o	+	↗	→

o Any survey ↘ Decrease
 + High ↗ Increase
 - Low → Stable

5

Table 4: Functioning indicators used to survey morphodynamic adjustments in Rohrschollen artificial side channel. Metrics, methods and evolutionary trend are summarized as a management toolkit to monitor the restoration-related changes. Long-term means >10 yr.

5.3 Guidelines to improve restoration efficiency and sustainability

10 Restoration efficiency can be assessed by using functioning indicators (Rinaldi *et al.*, 2017). Such indicators allow investigators to (1) determine the optimal functioning considering the targeted restoration goals (indicators should be used to define quantifiable restoration objectives, and to implement the pre-restoration survey), (2) assess morphological adjustments and identify the controlling factors, and (3) help make the restoration action more sustainable. Managers are thus encouraged to use a set of functioning indicators to monitor long-term post-restoration changes, in order to check if the

15 restoration effects are sustainable and, if not, to engage in a subsequent restoration step (if possible). Thus, indicators are useful to monitor processes at different spatial and temporal scales to follow changes but also to adapt management principles if needed. The indicators developed in our study contribute to the construction of an easily reproducible,

transposable (for current or future restoration) and transferable (to managers) toolbox, as suggested by Fryirs *et al.* (2018) or Díaz-Redondo *et al.* (2018). This is essential to assess both the efficiency and sustainability of any restoration. Using both geodetic and geomorphological surveys makes the monitoring strongly relevant, especially in case of a process-based restoration for which morphological dynamics are intense and frequent. In this context, hybrid methods can provide an accurate understanding of morphodynamics and identify main controlling (and limiting) factors. Because the proposed monitoring program can be relatively time-consuming and costly, managers may also simplify it for annual surveys, and use the full set for accurate surveys that could be realized every 3 to 5 yr and/or after intense or long floods.

This study underlines the importance of self-forming channel processes through bank erosion and vertical adjustments (bedload dynamics, riffle-pool sequences, bars development, etc.), especially in the case of artificial side channels mimicking natural forms and functioning. Bank erosion favors (i) sediment supply to the channel (including the coarse fraction), (ii) frequent deposition and (iii) longitudinal and lateral diversification. This underscores that it is preferable to excavate artificial side channels composed by a thin layer of fine sediments, or allow dynamic floods to excavate new channels into the floodplain, rather than reactivating clogged palaeochannels mostly filled by large quantities of fine sediments that can even be polluted (Eschbach *et al.*, 2018). Consequently, it enhances ecological potential because bed grain size diversification, bedload dynamics and geomorphic unit evolution represent key processes for aquatic habitats (Beisel *et al.*, 1998; Riquier *et al.*, 2017), especially in restored channels (Morandi *et al.*, 2014, Fryirs *et al.*, 2018). All these processes are favored by logjams, which in turn may intensify, and/or be intensified by, bank erosion (Beechie *et al.*, 2010; Stammel *et al.*, 2011; Choné and Biron, 2016). In any case, taking into account long-term temporal trajectories (>10 yr) can help in identifying areas for which potential post-restoration adjustments may be significantly different (areas composed by relatively small or large grain size). This should improve defining restoration targets and help interpreting post-restoration evolution thanks to morphodynamic indicators.

Indicators could help identifying sources of weaknesses in long-term functioning related to process-based restoration, for example, a deficit in the sediment budget or an area where erosion rates are particularly high. This raises the question of potential gravel augmentation, which is one of the main limitations of the kind of projects studied in this paper, especially in terms of management cost and sustainability (Harvey *et al.*, 2005).

6 Conclusion and perspectives

Two major outcomes are obtained in our study. First, the results showed that TLS and SfM-photogrammetry are relevant techniques to monitor morphological changes in fluvial environments, especially for large river side channels. SfM-photogrammetry is recommended for its cost and the flexibility of the acquisition, especially in dynamic side channels showing important and rapid changes. Producing and comparing complete 3-D models by combining terrestrial point clouds with bathymetric data provide a reliable way to identify and assess accurately morphological changes following floods at different spatial scales. Second, we demonstrate the importance of combining geodetic tools with geomorphical methods to develop straightforward morphodynamic indicators able to capture morphodynamic adjustments and processes. This is relevant for assessing both efficiency and sustainability of restoration projects. Indeed, monitoring fluvial changes in restoration activities requires using relevant functioning indicators, which should be determined in the early steps of restoration projects to define specific quantifiable objectives. Such indicators allow investigators to (i) monitor short- (<5 yr) and mid-/long- (at least 5 or >10 yr) term morphological changes, (ii) determine on this basis if the objectives are achieved and over which temporal scale, and (iii) allow inter-project comparison. As 1-D or 2-D hydraulic and morpho-sedimentary modelling is an increasingly used tool to predict changes and support manager decisions, it seems relevant that these modelling approaches integrate the proposed functioning indicators. In the case of an alluvial artificial side channel with water depths less than 2 m, topographic/bathymetric LIDAR should strengthen bathymetric datasets and simultaneously reduce the duration of field work.

7 Acknowledgments

This research was funded by the European Community (LIFE08 NAT/F/00471), the City of Strasbourg, the French National Center for Scientific Research (CNRS), the ZAEU (Zone Atelier Environnementale Urbaine - LTER), the Water Rhin-Meuse Agency, the DREAL Alsace, the “Région Alsace”, the “Département du Bas-Rhin” and the company “Électricité de France”. The authors would like to thank Stoil Chapkanski, Alexandre Hubeny, Léa Keiser and Jordane Serouilou for field assistance as well as Etienne Supper and Julie Roy for fieldwork and data processing. We also thank the two anonymous reviewers who provided very constructive comments that greatly contributed to improve the manuscript.

8 References

- Arnaud, F., Piégay, H., Vaudor, L., Bultingaire, L., Fantino, G., 2015. Technical specifications of low-frequency radio identification bedload tracking from field experiments: Differences in antennas, tags and operators. In *Geomorphology* 238, 37–46. doi:10.1016/j.geomorph.2015.02.029
- 5 Bangen, S., Wheaton, J., Bouwes, N., Jordan, C., Volk, C., Ward, M.B., 2014a. Crew variability in topographic surveys for monitoring wadeable streams: a case study from the Columbia River Basin. In *Earth Surface Processes and Landforms* 39, 2070–2086. doi:10.1002/esp.3600
- Bangen, S.G., Wheaton, J.M., Bouwes, N., Bouwes, B., Jordan, C., 2014b. A methodological intercomparison of topographic survey techniques for characterizing wadeable streams and rivers. In *Geomorphology* 206, 343–361.
10 doi:10.1016/j.geomorph.2013.10.010
- Barker, R., Dixon, L., Hooke, J., 1997. Use of terrestrial photogrammetry for monitoring and measuring bank erosion. In *Earth Surface Processes and Landforms* 22, 1217–1227.
- Beechie, T.J., Sear, D.A., Olden, J.D., Pess, G.R., Buffington, J.M., Moir, H., Roni, P., Pollock, M.M., 2010. Process-based principles for restoring river ecosystems. In *BioScience* 60, 209–222.
- 15 Beisel, J.-N., Usseglio-Polatera, P., Thomas, S., Moreteau, J.-C., 1998. Stream community structure in relation to spatial variation: the influence of mesohabitat characteristics. In *Hydrobiologia* 389, 73–88.
- Belletti, B., Rinaldi, M., Buijse, A.D., Gurnell, A.M., Mosselman, E., 2014. A review of assessment methods for river hydromorphology. In *Environmental Earth Sciences* 73, 2079–2100. doi:10.1007/s12665-014-3558-1
- Belletti, B., Rinaldi, M., Bussetini, M., Comiti, F., Gurnell, A.M., Mao, L., Nardi, L., Vezza, P., 2017. Characterising
20 physical habitats and fluvial hydromorphology: A new system for the survey and classification of river geomorphic units. In *Geomorphology* 283, 143–157. doi:10.1016/j.geomorph.2017.01.032
- Berger, A.R., 1997. Assessing rapid environmental change using geoindicators. In *Environmental Geology* 32, 36–44.
- Bernhardt, E.S., Palmer, M.A., Allan, J.D., Alexander, G., Barnas, K., Brooks, S., Carr, J., Clayton, S., Dahm, C., Follstad-Shah, J., others, 2005. Synthesizing US river restoration efforts. In *Science* 308, 636–637.

- Bizzi, S., Demarchi, L., Grabowski, R.C., Weissteiner, C.J., Van de Bund, W., 2016. The use of remote sensing to characterise hydromorphological properties of European rivers. *Aquatic sciences*. 78(1), pp. 57–70. doi:10.1007/s00027-015-0430-7
- Boike, J., Yoshikawa, K., 2003. Mapping of periglacial geomorphology using kite/balloon aerial photography. In *Permafrost and Periglacial Processes* 14, 81–85. doi:10.1002/ppp.437
- Brasington, J., Rumsby, B.T., McVey, R.A., 2000a. Monitoring and modelling morphological change in a braided gravel-bed river using high resolution GPS-based survey. In *Earth Surface Processes and Landforms* 25, 973–990. doi:10.1002/1096-9837(200008)25:9<973::AID-ESP111>3.0.CO;2-Y
- Brasington, J., Rumsby, B.T., McVey, R.A., 2000b. Monitoring and modelling morphological change in a braided gravel-bed river using high resolution GPS-based survey. In *Earth Surface Processes and Landforms* 25, 973–990.
- Brasington, J., Langham, J., Rumsby, B., 2003. Methodological sensitivity of morphometric estimates of coarse fluvial sediment transport. *Geomorphology*. 53(3–4), pp. 299–316. doi:10.1016/S0169-555X(02)00320-3
- Brierley, G.J., Fryirs, K.A., 2008. *River Futures: An Integrative Scientific Approach to River Repair*. Island Press, 325 p.
- Buchanan, B.P., Walter, M.T., Nagle, G.N., Schneider, R.L., 2012. Monitoring and assessment of a river restoration project in central New York. In *River Research and Applications* 28, 216–233. doi:10.1002/rra.1453
- Casado, M., Gonzalez, R., Kriechbaumer, T., Veal, A., 2015. Automated Identification of River Hydromorphological Features Using UAV High Resolution Aerial Imagery. In *Sensors* 15, 27969–27989. doi:10.3390/s151127969
- Chandler, J., Ashmore, P., Paola, C., Gooch, M., Varkaris, F., 2002. Monitoring River-Channel Change Using Terrestrial Oblique Digital Imagery and Automated Digital Photogrammetry. In *Annals of the Association of American Geographers* 92, 631–644. doi:10.1111/1467-8306.00308
- Chandler, J.H., Shiono, K., 2001. Measuring flume surfaces for hydraulics research using a Kodak DCS460. In *Photogrammetric record* 17, 39–61.
- Chapuis, M., Bright, C.J., Hufnagel, J., MacVicar, B., 2014. Detection ranges and uncertainty of passive Radio Frequency Identification (RFID) transponders for sediment tracking in gravel rivers and coastal environments. In *Earth Surface Processes and Landforms* 39, 2109–2120. doi:10.1002/esp.3620

- Chapuis, M., Dufour, S., Provansal, M., Couvert, B., de Linares, M., 2015. Coupling channel evolution monitoring and RFID tracking in a large, wandering, gravel-bed river: Insights into sediment routing on geomorphic continuity through a riffle–pool sequence. In *Geomorphology* 231, 258–269. doi:10.1016/j.geomorph.2014.12.013
- Chardon, V., Schmitt, L., Arnaud, F., Piégay, H., Clutier, A., under review, in revision. Efficiency and sustainability of gravel augmentation to restore large regulated rivers: insights from three experiments on the Rhine River (France/Germany). In *Geomorphology*.
- 5
- Choné, G., Biron, P.M., 2016. Assessing the Relationship Between River Mobility and Habitat. In *River Research and Applications* 32, 528–539. doi:10.1002/rra.2896
- CIPR-ICPR, 2012. Plan d’action contre les inondations 1995 - 2010 : objectifs opérationnels, mise en oeuvre et résultats - Bilan synthétique. Coblence.
- 10
- Collins, S., Moon, G., 1979. Stereometric Measurement of Streambank Erosion. In *Photogrammetric Engineering and Remote Sensing* 45, 183–190.
- Cook, K.L., 2017. An evaluation of the effectiveness of low-cost UAVs and structure from motion for geomorphic change detection. In *Geomorphology*. **278** pp. 195–208. doi:10.1016/j.geomorph.2016.11.009
- 15
- Corbonnois, J., Jacquemot, T., Giovannacci, L., Beck, T., Ghachi, M.E., 2011. Les indicateurs de l’évolution actuelle des lits fluviaux. Etude de cours d’eau du Nord-Est de la France. In *Revue Géographique de l’Est* 51, 17 p.
- Díaz-Redondo, M., Egger, G., Marchamalo, M., Damm, C., de Oliveira, R.P., Schmitt, L., 2018. Targeting lateral connectivity and morphodynamics in a large river-floodplain system: The upper Rhine River: morphodynamic recovery in the Upper Rhine river. *River research and applications*. . doi:10.1002/rra.3287
- 20
- Dickinson, W., Scott, A., 1979. Analysis of Streambank Erosion Variables. In *Canadian Agricultural Engineering* 21, 19–25.
- Dietrich, J.T., 2016. Riverscape mapping with helicopter-based Structure-from-Motion photogrammetry. In *Geomorphology* 252, 144–157. doi:10.1016/j.geomorph.2015.05.008
- 25
- Downs, P.W., Kondolf, G.M., 2002. Post-Project Appraisals in Adaptive Management of River Channel Restoration. In *Environmental Management* 29, 477–496. doi:10.1007/s00267-001-0035-X
- Dufour, S., Piégay, H., 2009. From the myth of a lost paradise to targeted river restoration: forget natural references and focus on human benefits. In *River Research and Applications* 25, 568–581. doi:10.1002/rra.1239

- Eltner, A., Kaiser, A., Castillo, C., Rock, G., Neugirg, F., Abellán, A., 2016. Image-based surface reconstruction in geomorphometry: merits, limits and developments. *Earth surface dynamics*. 4(2), pp. 359–389. doi:10.5194/esurf-4-359-2016
- Eschbach, D., Piasny, G., Schmitt, L., Pfister, L., Grussenmeyer, P., Koehl, M., Skupinski, G., Serradj, A., 2017. Thermal-infrared remote sensing of surface water-groundwater exchanges in a restored anastomosing channel (Upper Rhine River, France). In *Hydrological Processes* 31, 1113–1124. doi:10.1002/hyp.11100
- Eschbach, D., Schmitt, L., Imfeld, G., Preusser, F., Payraudeau, S., May, J.-H., Trauerstein, M., Skupinski, G., 2018. Long-term trajectories of rivers to perform functional restorations: an interdisciplinary case study on the Rhine River (Rohrschollen Island, France). *Hydrology and earth system sciences*. 22 pp. 2717–2737. doi:https://doi.org/10.5194/hess-22-2717-2018
- ESSA (2016), Specializing in environmental sciences and decision support, River Bathymetry Toolkit (RBT) <http://essa.com/tools/river-bathymetry-toolkit-rbt/>
- Fausch, K.D., Torgersen, C.E., Baxter, C.V., Li, H.W., 2002. Landscapes to Riverscapes: Bridging the Gap between Research and Conservation of Stream Fishes. In *BioScience* 52, 483. doi:10.1641/0006-3568(2002)052[0483:LTRBTG]2.0.CO;2
- Ferguson, R.I., Ashmore, P.E., Ashworth, P.J., Paola, C., Prestegard, L., 1992. Measurements in a braided river Chute and Lobe: 1. Flow pattern, sediment transport and channel change. In *Water Resources Research* 28, 1877–1886.
- Fonstad, M.A., Dietrich, J.T., Courville, B.C., Jensen, J.L., Carbonneau, P.E., 2013. Topographic structure from motion: a new development in photogrammetric measurement. In *Earth Surface Processes and Landforms* 38, 421–430. doi:10.1002/esp.3366
- Formann, E., Habersack, H.M., Schober, S., 2007. Morphodynamic river processes and techniques for assessment of channel evolution in Alpine gravel bed rivers. In *Geomorphology* 90, 340–355. doi:10.1016/j.geomorph.2006.10.029
- Fryirs, K.A., Brierley, G.J., Hancock, F., Cohen, T.J., Brooks, A.P., Reinfelds, I., Cook, N., Raine, A., 2018. Tracking geomorphic recovery in process-based river management. *Land degradation & development*. 29(9), pp. 3221–3244. doi:10.1002/ldr.2984
- Fuller, I.C., Large, A.R.G., Milan, D.J., 2003. Quantifying channel development and sediment transfer following chute cutoff in a wandering gravel-bed river. In *Geomorphology* 54, 307–323. doi:10.1016/S0169-555X(02)00374-4

- Gao, J., 2009. Bathymetric mapping by means of remote sensing: methods, accuracy and limitations. *Progress in physical geography: earth and environment*. 33(1), pp. 103–116. doi:10.1177/0309133309105657
- Grussenmeyer, P., Landes, T., Doneus, M., Lerma, J.-L., 2016. Basics of range-based modelling techniques in Cultural Heritage (Chapter pp. 305-368). In: *3D Recording, Documentation and Management of Cultural Heritage*, Publisher: Whittles Publishing, Editors: Efstratios Stylianidis, Fabio Remondino, 388 pages, ISBN 978-184995-168-5
- Grussenmeyer, P., Perdrizet, F., 1996. Archeological Photogrammetry with small format cameras: the survey of the forum vetus in Sarmizegetusa (Romania). *International archives of Photogrammetry and Remote Sensing*, Vienna, 9-19 July 1996. ISSN 0256-1840, Vol. XXXI Part B5, p200-204.
- Gurnell, A.M., Morrissey, I.P., Boitsidis, A.J., Bark, T., Clifford, N.J., Petts, G.E., Thompson, K., 2006. Initial Adjustments Within a New River Channel: Interactions Between Fluvial Processes, Colonizing Vegetation, and Bank Profile Development. In *Environmental Management* 38, 580–596. doi:10.1007/s00267-005-0190-6
- Harvey, B., McBain, S., Reiser, D., Rempel, L., Sklar, L., Lave, R., 2005. Key uncertainties in gravel augmentation: geomorphological and biological research needs for effective river restoration (CAFED Science and Ecosystem Restoration Programs). Sacramento, USA pp. 92.
- Hassan, M.A., Bradley, D.N., 2017. Geomorphic Controls on Tracer Particle Dispersion in Gravel-Bed Rivers Tsutsumi, Daizo, Laronne, Jonathan B. (Eds.), In *Gravel-bed rivers*. John Wiley & Sons, Ltd, Chichester, UK, pp. 159–184 doi:10.1002/9781118971437.ch6
- Heritage, G., Fuller, I., Charlton, M., Brewer, P., Passmore, D., 1998. CDW photogrammetry of low relief fluvial features: accuracy and implications for reach-scale sediment budgeting. In *Earth Surface Processes and Landforms* 23, 1219–1233.
- Hickin, E.J., 1983. River Channel Changes: Retrospect and Prospect, in: Collinson, J.D., Lewin, J. (Eds.), *Modern and Ancient Fluvial Systems*. Blackwell Publishing Ltd., pp. 59–83, 59–83p.
- James, M.R., Robson, S., 2012. Straightforward reconstruction of 3D surfaces and topography with a camera: Accuracy and geoscience application. *Journal of geophysical research: earth surface*. 117(F3), 17 p. doi:10.1029/2011JF002289
- Javernick, L., Brasington, J., Caruso, B., 2014. Modeling the topography of shallow braided rivers using Structure-from-Motion photogrammetry. In *Geomorphology* 213, 166–182. doi:10.1016/j.geomorph.2014.01.006

- Jozkow, G., Borkowski, A., Kasprzak, M., 2016. Monitoring of fluvial transport in the mountain river bed using terrestrial laser scanning. In *ISPRS - International Archives of the Photogrammetry, Remote Sensing and Spatial Information Sciences XLI-B7*, 523–528. doi:10.5194/isprsarchives-XLI-B7-523-2016
- Jugie, M., Gob, F., Vermoux, C., Brunstein, D., Tamisier, V., Le Coeur, C., Grancher, D., 2018. Characterizing and quantifying the discontinuous bank erosion of a small low energy river using Structure-from-Motion Photogrammetry and erosion pins. *Journal of hydrology*. 563 pp. 418–434. doi:10.1016/j.jhydrol.2018.06.019
- Kondolf, G.M., 2016. Tools in Fluvial Geomorphology. John Wiley & Sons, 569 p.
- Kuo, C.-W., Brierley, G., Chang, Y.-H., 2015. Monitoring channel responses to flood events of low to moderate magnitudes in a bedrock-dominated river using morphological budgeting by terrestrial laser scanning. In *Geomorphology* 235, 1–14. doi:10.1016/j.geomorph.2015.01.019
- Lague, D., Brodu, N., Leroux, J., 2013. Accurate 3D comparison of complex topography with terrestrial laser scanner: Application to the Rangitikei canyon (N-Z). In *ISPRS Journal of Photogrammetry and Remote Sensing* 82, 10–26. doi:10.1016/j.isprsjprs.2013.04.009
- Lamarre, H., Mac Vicar, B., Roy, A.G., 2005. Using Passive Integrated Transponder (PIT) Tags to Investigate Sediment Transport in Gravel-Bed Rivers. In *Journal of Sedimentary Research* 75, 736–741.
- Lamarre, H., Roy, A.G., 2008. The role of morphology on the displacement of particles in a step–pool river system. In *Geomorphology* 99, 270–279. doi:10.1016/j.geomorph.2007.11.005
- Lane, S.N., Chandler, J.H., Porfiri, K., 2001. Monitoring river channel and flume surfaces with digital photogrammetry. In *Journal of Hydraulic Engineering* 127, 871–877.
- Lane, S.N., James, T.D., Crowell, M.D., 2000. Application of digital photogrammetry to complex topography for geomorphological research. In *Photogrammetric record* 16, 793–821.
- Lane, S.N., Richards, K.S., Chandler, J.H., 1994. Developments in monitoring and modelling small-scale river bed topography. In *Earth Surface Processes and Landforms* 19, 349–368.
- Lane, S.N., Westaway, R.M., Murray Hicks, D., 2003. Estimation of erosion and deposition volumes in a large, gravel-bed, braided river using synoptic remote sensing. *Earth surface processes and landforms*. 28(3), pp. 249–271. doi:10.1002/esp.483

- Legleiter, C.J., 2012. Remote measurement of river morphology via fusion of LiDAR topography and spectrally based bathymetry. In *Earth Surface Processes and Landforms* 37, 499–518. doi:10.1002/esp.2262
- Lejot, J., Delacourt, C., Piégay, H., Fournier, T., Trémélo, M.-L., Allemand, P., 2007. Very high spatial resolution imagery for channel bathymetry and topography from an unmanned mapping controlled platform. In *Earth Surface Processes and Landforms* 32, 1705–1725. doi:10.1002/esp.1595
- MacVicar, B., Chapuis, M., Buckrell, E., Roy, A., 2015. Assessing the Performance of In-Stream Restoration Projects Using Radio Frequency Identification (RFID) Transponders. In *Water* 7, 5566–5591. doi:10.3390/w7105566
- MacWilliams, M.L., Wheaton, J.M., Pasternack, G.B., Street, R.L., Kitanidis, P.K., 2006. Flow convergence routing hypothesis for pool-riffle maintenance in alluvial rivers. In *Water Resources Research* 42. doi:10.1029/2005WR004391
- 10 Malavoi, J.R., Souchon, Y., 2002. Description standardisée des principaux faciès d'écoulement observables en rivière: clé de détermination qualitative et mesures physiques. In *Bulletin Fr. Pêche Pisciculture* 365/366, 367–372.
- Malavoi, J.R., Bravard, J.P., 2010. *Eléments d'hydrogéomorphologie fluviale*. Rapport ONEMA. 228 p.
- Marteau, B., Vericat, D., Gibbins, C., Batalla, R.J., Green, D.R., 2017. Application of Structure-from-Motion photogrammetry to river restoration: Application of SfM Photogrammetry to River Restoration. *Earth surface processes and landforms*. 42(3), pp. 503–515. doi:10.1002/esp.4086
- 15
- Martin, Y., Church, M., 1995. Bed-material transport estimated from channel surveys: Vedder River, British Columbia. In *Earth Surface Processes and Landforms* 20, 347–361.
- McLean, D.G., Church, M., 1999. Sediment transport along lower Fraser River: 2. Estimates based on the long-term gravel budget. In *Water Resources Research* 35, 2549–2559. doi:10.1029/1999WR900102
- 20 Milan, D.J., 2012. Geomorphic impact and system recovery following an extreme flood in an upland stream: Thinhope Burn, northern England, UK. In: *Geomorphology* 138, 319–328. doi:10.1016/j.geomorph.2011.09.017
- Milan, D.J., Large, A.R.G., 2014. Magnetic tracing of fine-sediment over pool-riffle morphology. In: *CATENA* 115, 134–149. doi:10.1016/j.catena.2013.11.003
- Morandi, B., Piégay, H., Lamouroux, N., Vaudor, L., 2014. How is success or failure in river restoration projects evaluated? Feedback from French restoration projects. In: *Journal of Environmental Management* 137, 178–188. doi:10.1016/j.jenvman.2014.02.010
- 25

- Murtiyoso, A., Grussenmeyer, P., 2017. Documentation of Heritage Buildings using Close Range UAV Images: Dense Matching Issues, Comparison, and Case Studies. In: *The Photogrammetric Record, an International Journal of Photogrammetry* 32: 206–229. doi:10.1111/phor.12197
- Nadal-Romero, E., Revuelto, J., Errea, P., López-Moreno, J.I., 2015. The application of terrestrial laser scanner and SfM photogrammetry in measuring erosion and deposition processes in two opposite slopes in a humid badlands area (central Spanish Pyrenees). In *SOIL* 1, 561–573. doi:10.5194/soil-1-561-2015
- Nielsen, S.N., Jørgensen, S.E., 2013. Goal functions, orientors and indicators (GoFOrit's) in ecology. Application and functional aspects – Strengths and weaknesses. *Ecological indicators*. 28 pp. 31–47. doi:10.1016/j.ecolind.2012.12.015
- Painter, R.B., Blyth, K., Mosedale, J.C., Kelly, M., 1974. The effect of afforestation on erosion processes and sediment yield. In *Effects of Man on the Interface of the Hydrological Cycle with the Physical Environment*, 62–67.
- Palmer, M.A., Bernhardt, E.S., Allan, J.D., Lake, P.S., Alexander, G., Brooks, S., Carr, J., Clayton, S., Dahm, C.N., Follstad Shah, J., Galat, D.L., Loss, S.G., Goodwin, P., Hart, D.D., Hassett, B., Jenkinson, R., Kondolf, G.M., Lave, R., Meyer, J.L., O'Donnell, T.K., Pagano, L., Sudduth, E., 2005. Standards for ecologically successful river restoration: Ecological success in river restoration. In *Journal of Applied Ecology* 42, 208–217. doi:10.1111/j.1365-2664.2005.01004.x
- Palmer, M.A., Menninger, H.L., Bernhardt, E., 2010. River restoration, habitat heterogeneity and biodiversity: a failure of theory or practice? In *Freshwater Biology* 55, 205–222. doi:10.1111/j.1365-2427.2009.02372.x
- Pander, J., Geist, J., 2013. Ecological indicators for stream restoration success. In *Ecological indicators*. 30 pp. 106–118. doi:10.1016/j.ecolind.2013.01.039
- Prosdocimi, M., Calligaro, S., Sofia, G., Dalla Fontana, G., Tarolli, P., 2015. Bank erosion in agricultural drainage networks: new challenges from structure-from-motion photogrammetry for post-event analysis. *Earth surface processes and landforms*. 40(14), pp. 1891–1906. doi:10.1002/esp.3767
- Pyle, C.J., Richards, K.S., Chandler, J.H., 1997. Digital Photogrammetric Monitoring of River Bank Erosion. In *The Photogrammetric Record* 15, 753–764. doi:10.1111/0031-868X.00083
- Raclot, D., Puech, C., Mathys, N., Roux, B., Jacome, A., Asseline, J., Bailly, J.-S., 2005. Photographies aériennes prises par drone et Modèle Numérique de Terrain : apports pour l'observatoire sur l'érosion de Draix. *Géomorphologie : relief, processus, environnement*. 11(1), pp. 7–20. doi:10.4000/geomorphologie.209

- Raven, P.J., Holmes, N.T.H., Charrier, P., Dawson, F.H., Naura, M., Boon, P.J., 2002. Towards a harmonized approach for hydromorphological assessment of rivers in Europe: a qualitative comparison of three survey methods. In *Aquatic Conservation: Marine and Freshwater Ecosystems* 12, 405–424. doi:10.1002/aqc.536
- Rayburg, S., Thoms, M., Neave, M., 2009. A comparison of digital elevation models generated from different data sources.
5 In *Geomorphology* 106, 261–270. doi:10.1016/j.geomorph.2008.11.007
- Remondino, F., El-Hakim, S., 2006. Image based 3D modelling: a review. In *The Photogrammetric Record* 21, 269–291.
- Rinaldi, M., Belletti, B., Bussettini, M., Comiti, F., Golfieri, B., Lastoria, B., Marchese, E., Nardi, L., Surian, N., 2017. New tools for the hydromorphological assessment and monitoring of European streams. *Journal of environmental management*. 202 pp. 363–378. doi:10.1016/j.jenvman.2016.11.036
- 10 Riquier, J., Piégay, H., Lamouroux, N., Vaudor, L., 2017. Are restored side channels sustainable aquatic habitat features? Predicting the potential persistence of side channels as aquatic habitats based on their fine sedimentation dynamics. *Geomorphology*. 295 pp. 507–528. doi:10.1016/j.geomorph.2017.08.001
- Schmitt, L., Maire, G., Nobelis, P., Humbert, J., 2007. Quantitative morphodynamic typology of rivers: a methodological study based on the French Upper Rhine basin. In *Earth Surface Processes and Landforms* 32, 1726–1746.
15 doi:10.1002/esp.1596
- Schmitt, L., Lafont, M., Trèmolières, M., Jezequel, C., Vivier, A., Breil, P., Namour, P., Valin, K., Valette, L., 2011. Using hydro-geomorphological typologies in functional ecology: Preliminary results in contrasted hydrosystems. In *Physics and Chemistry of the Earth, Parts A/B/C* 36, 539–548. doi:10.1016/j.pce.2009.11.011
- Schneider, J., Hegglin, R., Meier, S., Turowski, J.M., Nitsche, M., Rickenmann, D., 2010. Studying sediment transport in
20 mountain rivers by mobile and stationary RFID antennas, in: Ditttrich, Koll, Aberle & Geisenhainer (Eds). *River Flow 2010: Proceedings of the International Conference on Fluvial Hydraulics*. Ditttrich, Koll, Aberle & Geisenhainer (Eds), 8 p.
- Schumm S-A., 1968. Sinuosity of alluvial rivers in the Great Plains. *Bull. geol. soc. america*. 74 pp. 1089–1100.
- Sear, D.A., 1996. Sediment transport processes in pool–riffle sequences. In *Earth Surface Processes and Landforms* 21, 241–262.
- 25 Smith, M.J., Chandler, J., Rose, J., 2009. High spatial resolution data acquisition for the geosciences: kite aerial photography. In *Earth Surface Processes and Landforms* 34, 155–161. doi:10.1002/esp.1702

- Smith, M.W., Carrivick, J.L., Quincey, D.J., 2016. Structure from motion photogrammetry in physical geography. *Progress in physical geography*. 40(2), pp. 247–275. doi:10.1177/0309133315615805
- Stammel, B., Cyffka, B., Geist, J., Müller, M., Pander, J., Blasch, G., Fischer, P., Gruppe, A., Haas, F., Kilg, M., Lang, P., Schopf, R., Schwab, A., Utschik, H., Weißbrod, M., 2011. Floodplain restoration on the Upper Danube (Germany) by re-
5 establishing water and sediment dynamics: a scientific monitoring as part of the implementation. *River systems*. 20(1–2), pp. 55–70. doi:10.1127/1868-5749/2011/020-0033
- Telling, J., Lyda, A., Hartzell, P., Glennie, C., 2017. Review of Earth science research using terrestrial laser scanning. *Earth-science reviews*. 169 pp. 35–68. doi:10.1016/j.earscirev.2017.04.007
- TI-RFID, 2006. Eco-line 23 mm glass transponder, RI-TRP-REHP (read only), RI-TRPWEHP (read/write), reference guide,
10 Texas Instruments. <http://www.ti.com/lit/ug/scbu034/scbu034.pdf> (16.01.2014), n.d.
- Vericat, D., Brasington, J., Wheaton, J., Cowie, M., 2009. Accuracy assessment of aerial photographs acquired using lighter-than-air blimps: low-cost tools for mapping river corridors. In *River Research and Applications* 25, 985–1000. doi:10.1002/rra.1198
- Westaway, R.M., Lane, S.N., Hicks, D.M., 2003. Remote survey of large-scale braided, gravel-bed rivers using digital
15 photogrammetry and image analysis. In *International Journal of Remote Sensing* 24, 795–815. doi:10.1080/01431160110113070
- Westaway, R.M., Lane, S.N., Hicks, D.M., 2000. The development of an automated correction procedure for digital photogrammetry for the study of wide, shallow, gravel-bed rivers. In *Earth Surface Processes and Landforms* 25, 209–226.
- Westoby, M.J., Brasington, J., Glasser, N.F., Hambrey, M.J., Reynolds, J.M., 2012. “Structure-from-Motion”
20 photogrammetry: A low-cost, effective tool for geoscience applications. In *Geomorphology* 179, 300–314. doi:10.1016/j.geomorph.2012.08.021
- Wheaton, J.M., Brasington, J., Darby, S.E., Sear, D.A., 2009. Accounting for uncertainty in DEMs from repeat topographic surveys: improved sediment budgets. In *Earth Surface Processes and Landforms*, pp. 136-156. doi:10.1002/esp.1886
- Williams, R.D., Brasington, J., Vericat, D., Hicks, D.M., 2014. Hyperscale terrain modelling of braided rivers: fusing mobile
25 terrestrial laser scanning and optical bathymetric mapping: Hyperscale terrain modelling of braided rivers. *Earth surface processes and landforms*. 39(2), pp. 167–183. doi:10.1002/esp.3437

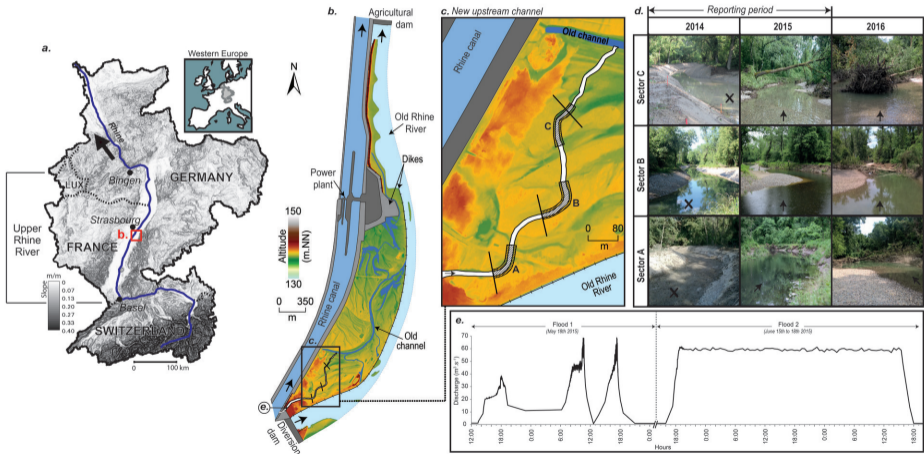
Wolman, M.G., 1954. A method of sampling coarse river-bed material. In *transactions, American Geophysical union* 35, 951–956.

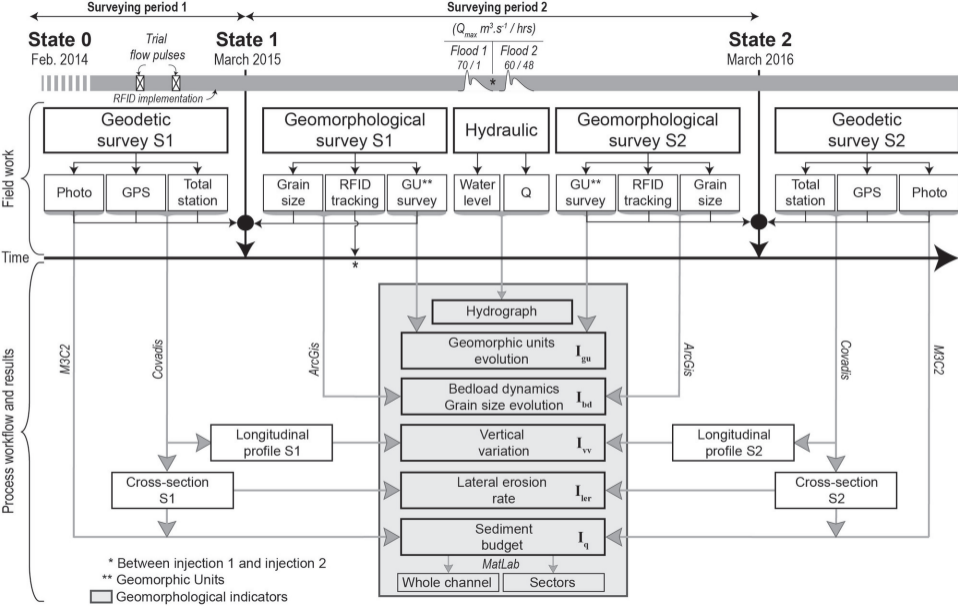
Woodget, A.S., Carbonneau, P.E., Visser, F., Maddock, I.P., 2015. Quantifying submerged fluvial topography using hyperspatial resolution UAS imagery and structure from motion photogrammetry. *Earth surface processes and landforms*. 40(1), pp. 47–64. doi:10.1002/esp.3613

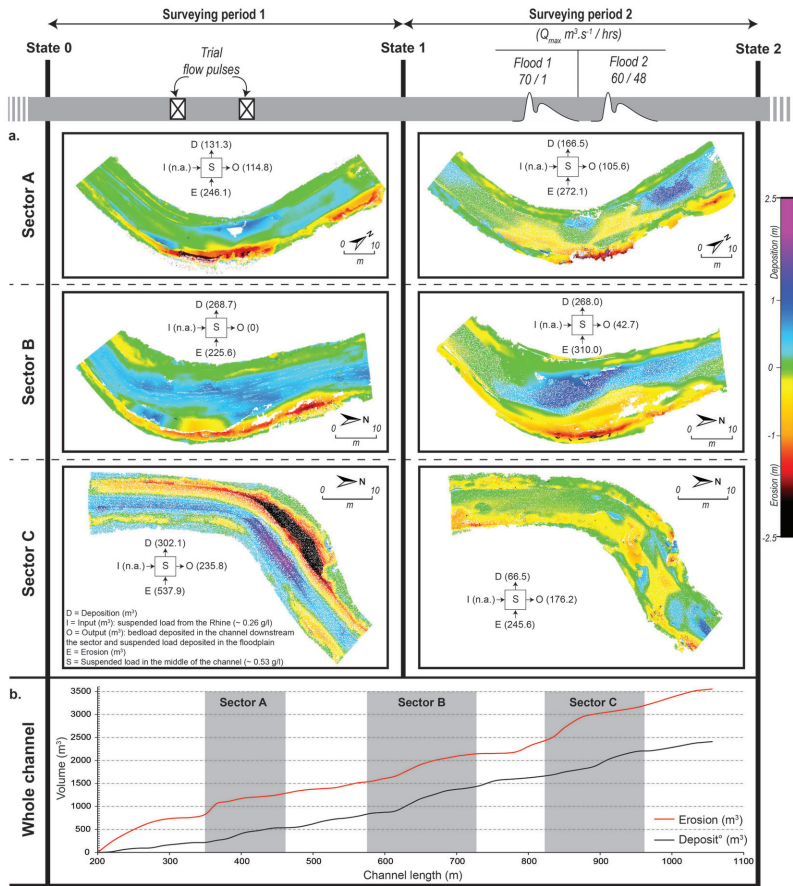
Woolsey, S., Capelli, F., Gonser, T., Hoehn, E., Hostmann, M., Junker, B., Paetzold, A., Roulier, C., Schweizer, S., Tiegs, S.D., Tockner, K., Weber, C., Peter, A., 2007. A strategy to assess river restoration success. *Freshwater biology*. 52(4), pp. 752–769. doi:10.1111/j.1365-2427.2007.01740.x


Wyrick, J.R., Pasternack, G.B., 2016. Revealing the natural complexity of topographic change processes through repeat surveys and decision-tree classification. *Earth surface processes and landforms*. 41(6), pp. 723–737. doi:10.1002/esp.3854

Wyrick, J.R., Senter, A.E., Pasternack, G.B., 2014. Revealing the natural complexity of fluvial morphology through 2D hydrodynamic delineation of river landforms. *Geomorphology*. 210 pp. 14–22. doi:10.1016/j.geomorph.2013.12.013

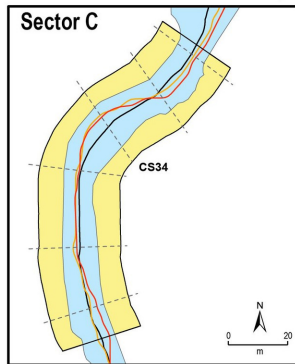
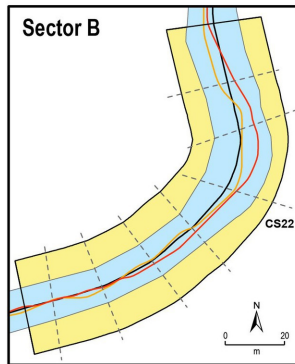
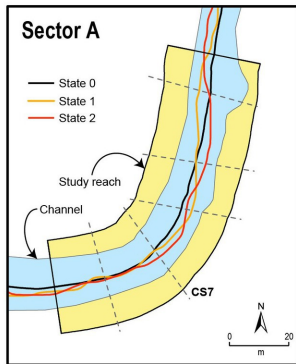




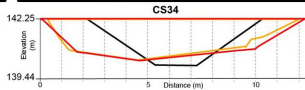
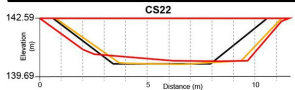
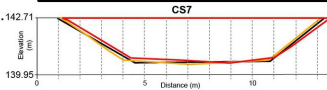


Flow direction 

a.

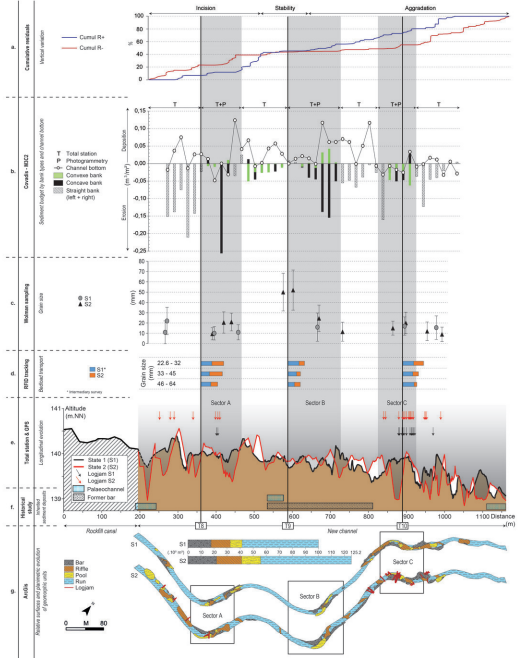


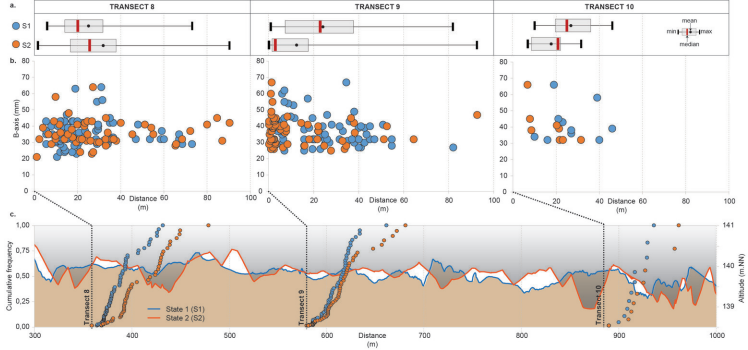
b.



c.

	State 0	State 1	State 2	State 0	State 1	State 2	State 0	State 1	State 2
Surface (m ²)	20.39	19.90	20.89	16.56	17.31	19.17	11.16	16.19	18.60
Width (m)	12.26	12.30	12.61	10.46	11.10	12.13	8.52	12.29	12.91
Average depth (m)	2.16	1.64	1.66	2.30	1.56	1.58	2.21	1.32	1.44
w/d	5.68	7.39	7.61	4.55	7.12	7.68	3.77	9.33	8.96
Specific stream power (W/m ²)	15.40	15.40	15.00	18.10	17.00	15.60	22.20	15.40	14.60
Lateral erosion (%)	0.3		2.5	6.1		9.3	44.2		5.0





Authors	Date	Context	Approach	Geomorphological dimensions & components						DEM methods		Hydromorphological methods						
				Channel types	River restoration	Lateral channel restoration	Geomorphological survey	Methodological studies ^a	Lateral adjustments	Vertical adjustments	Bedload dynamics	Hydrodynamics	Geomorphic units evolution	Lasergrammetry	Photogrammetry	Levelling (cross-section)	RFID tracking	Hydraulic modelling
Collins and Moon,	1979	WR		•							•							
Dickinson and Scott,	1979	MR		•							•							
Lane et al.,	1994	BR			•			•	•		•	•						
Martin and Church,	1995	BR		•				•	•			•						•
Barker et al.,	1997	MR			•			•			•							
Pyle et al.,	1997	PGR			•			•			•							
Heritage et al.,	1998	MR			•			•			•							
Westaway et al.,	2000	BR			•			•			•							
Brasington et al.,	2000	BR			•			•			•	•						
Chandler and Shiono,	2001	TF			•						•							
Lane et al.,	2001	TF			•						•							
Chandler et al.,	2002	PGR			•			•			•	•						
Fuller et al.,	2003	WR		•				•	•			•						•
Formann et al.,	2007	BR	•					•	•		•	•			•			
Lejot et al.,	2007	BR	•	•	•			•	•		•	•						• ^b
Wheaton et al.,	2009	BR			•			•			•	•	•					•
Lague et al.,	2013	MR			•			•			•							
Bangen et al.,	2014a	SAC			•			•				•						•
Javernick et al.,	2014	BR			•			•			•							
Casado et al.,	2015	WR			•			•			•							• ^c
Chapuis et al.,	2015	WR		•				•	•		•	•	•	•	•			
Kuo et al.,	2015	BR		•				•			•							•
MacVicar et al.,	2015	SAC	•		•							•		•				
Brunier et al.,	2016	BR		•				•			•							•
Dietrich,	2016	SAC	•	•	•			•	•		•	•	•					
Jozkow et al.,	2016	MS		•				•	•		•							
Belletti et al.,	2017	WR			•													• ^d
Marteau et al.,	2017	MS	•		•			•	•		•							•
Cook,	2017	WR			•			•	•		•	•						
Wyrick et al.,	2016	WR			•			•	•									• ^e
Jugie et al.,	2018	SAC		•				•	•		•	•						• ^f

BR Braiding River

SAC Small Alluvial Channel

TF Tilting Flume

MR Meandering River

MS Mountain Stream

PGR ProGlacial River

WR Wandering River

^a Results focused on methodological innovation (accuracy, methodological comparison...)

^b Bathymetric models

^c Unmanned Aerial Vehicles (UAV) and Artificial Neural Networks (ANN)

^d Geomorphic Units Survey (GUS) and Morphological Quality Index (MQI)

^e Near-census approach and decision-tree classification

^f Photo-Electronic Erosion Pin (PEEP)

	Sector A		Sector B		Sector C	
	Left bank	Right bank	Left bank	Right bank	Left bank	Right bank
Number of image	128	90	129	101	74	83
Number of GCP	5	6	7	8	10	7
Reprojection error <i>(Standard deviation m)</i>	0.001	0.02	0.02	0.05	0.03	0.01
Reprojection error <i>(Standard deviation pixels)</i>	0.18	0.23	0.49	0.2	0.19	0.12

Sector A	SP1	SP2	<i>Diff.</i>
Deposition (D)	131,3	166,5	35,2
Output (O)	114,8	105,6	-9,2
Erosion (E)	246,1	272,1	26

Sector B	SP1	SP2	<i>Diff.</i>
Deposition (D)	268,7	268	-0,7
Output (O)	0	42,7	42,7
Erosion (E)	225,6	310	84,4

Sector C	SP1	SP2	<i>Diff.</i>
Deposition (D)	302,1	66,5	-235,6
Output (O)	235,8	176,2	-59,6
Erosion (E)	537,9	245,6	-292,3

INDICATORS	NAME	METRICS	METHODS	State		Evolutionary trend	
				Initial state	Target	Post-Resto°	Long-term Target
Geomorphic units evolution	I_{gu}	Surfaces of geomorphic units (habitats)	Mapping of riffle, pool, run, logjams (GPS; ArcGis)	-	+	↗	→
Bedload dynamics	I_{bd}	Transport distances and dispersion	RFID tracking	○	+	↗	→
Vertical variation	I_w	Vertical evolution trend	{ Thalweg longitudinal profile Cumul of the residuals	-	+	↗	→
Lateral erosion	W/D I_{ler}	Width/depth ratio $I_{ler} = \left[\frac{w_e}{w_{in}} \right] * 100$	Cross section (Total Station)	-	+	↗	→
Sediment budget	I_q	Volumes (differences) of eroded and deposited sediments	TLS/SfM-photogrammetry/Total Station and DoD	○	+	↗	→

○ Any survey
+ High
- Low

↘ Decrease
↗ Increase
→ Stable